



Article

Scratching Beneath the Surface: A Model to Predict the Vertical Distribution of *Prochlorococcus* Using Remote Sensing

Priscila K. Lange ^{1,*} , Robert J. W. Brewin ^{2,3}, Giorgio Dall'Olmo ^{2,3}, Glen A. Tarran ² , Shubha Sathyendranath ^{2,3}, Mikhail Zubkov ⁴ and Heather A. Bouman ¹

¹ Department of Earth Sciences, University of Oxford, South Parks Rd, OX1 3AN Oxford, UK; heather.bouman@earth.ox.ac.uk

² Plymouth Marine Laboratory, Prospect Place, The Hoe, PL1 3DH Plymouth, UK; robr@pml.ac.uk (R.J.W.B.); gdal@pml.ac.uk (G.D.O.); gat@pml.ac.uk (G.A.T.); shubha.sathyendranath@dal.ca (S.S.)

³ National Centre for Earth Observation, Plymouth Marine Laboratory, PL1 3DH Plymouth, UK

⁴ National Oceanography Centre Southampton, Waterfront Campus, SO14 3ZH Southampton, UK; mvz@noc.ac.uk

* Correspondence: prilange@gmail.com

Received: 27 April 2018; Accepted: 18 May 2018; Published: 29 May 2018



Abstract: The unicellular cyanobacterium *Prochlorococcus* is the most dominant resident of the subtropical gyres, which are considered to be the largest biomes on earth. In this study, the spatial and temporal variability in the global distribution of *Prochlorococcus* was estimated in the Atlantic Ocean using an empirical model based on data from 13 Atlantic Meridional Transect cruises. Our model uses satellite-derived sea surface temperature (SST), remote-sensing reflectance at 443 and 488 nm, and the water temperature at a depth of 200 m from Argo data. The model divides the population of *Prochlorococcus* into two groups: *ProI*, which dominates under high-light conditions associated with the surface, and *ProII*, which favors low light found near the deep chlorophyll maximum. *ProI* and *ProII* are then summed to provide vertical profiles of the concentration of *Prochlorococcus* cells. This model predicts that *Prochlorococcus* cells contribute 32 Mt of carbon biomass (7.4×10^{26} cells) to the Atlantic Ocean, concentrated mainly within the subtropical gyres (35%) and areas near the Equatorial Convergence Zone (30%). When projected globally, 3.4×10^{27} *Prochlorococcus* cells represent 171 Mt of carbon biomass, with 43% of this global biomass allocated to the upper ocean (0–45 m depth). Annual cell standing stocks were relatively stable between the years 2003 and 2014, and the contribution of the gyres varies seasonally as gyres expand and contract, tracking changes in light and temperature, with lowest cell abundances during the boreal and austral winter (1.4×10^{13} cells m^{-2}), when surface cell concentrations were highest (9.8×10^4 cells mL^{-1}), whereas the opposite scenario was observed in spring–summer (2×10^{13} cells m^{-2}). This model provides a three-dimensional view of the abundance of *Prochlorococcus* cells, revealing that *Prochlorococcus* contributes significantly to total phytoplankton biomass in the Atlantic Ocean, and can be applied using either in situ measurements at the sea surface ($r^2 = 0.83$) or remote-sensing observables ($r^2 = 0.58$).

Keywords: *Prochlorococcus*; light dependency; deep biomass maximum; subtropical gyres; seasonality

1. Introduction

Until the early 1980s, the largest biomes on our planet, referred collectively as the subtropical gyres [1–3], were considered to be oceanic deserts as they are characterised by low biological primary productivity [4]. In the central subtropical gyres, extreme high-light conditions and low-nutrient concentrations hamper phytoplankton growth at the sea surface and lead to very low intracellular

pigment concentrations [5,6]. Yet, lying beneath this seemingly barren surface layer, a deep chlorophyll maximum (DCM) is commonly observed at depths between 80 to 120 m [7,8]. This peak in pigment concentration is the result of light penetrating sufficiently deep in the water column to reach depths where nutrients are available from deep reservoirs [9]. Cells found at this depth attain net growth by increasing their intracellular pigment concentration to thrive at low-light levels. The DCM is considered a ubiquitous feature of stratified subtropical waters [5,8]. This allocation of pigment biomass at depth makes these gyre biomes more similar to terrestrial savannahs than deserts. Like the subtropical gyres, savannahs have most of their biomass buried below ground, protected from harsh surface conditions [10]. Although the contribution of the DCM to the integrated chlorophyll biomass in the subtropical gyres is significant, it is still low when compared with coastal marine environments and shelf seas [8].

The use of shipboard flow cytometry revolutionised the study of small phytoplankton cells. In 1988, Chisholm, Olson, and colleagues [11] first documented a ubiquitous picocyanobacterium that was indistinguishable from other bacteria using traditional microscopy, but has since been discovered to be the most abundant photosynthetic organism in the oceans—*Prochlorococcus*. The average abundance of *Prochlorococcus* cells in subtropical and tropical waters [12–17] is roughly the same order of magnitude of most phytoplankton blooms where a single species of alga typically reaches cell abundances of 10^4 – 10^5 cells mL^{-1} [18]. Despite its minute size and corresponding low intracellular carbon content (~ 50 fg C cell $^{-1}$) [19], this single genus is numerically dominant over vast swaths of the global ocean, with global standing stocks in the order of 10^{27} cells [20,21] and makes an immense contribution to the marine organic carbon pool.

Although the quantification of *Prochlorococcus* cells by flow cytometry has increased our understanding of the contribution of this cyanobacterium to phytoplankton biomass in the subtropical gyres, data coverage in these vast regions remains poor. Optical sensors mounted on earth-orbiting satellites provide a synoptic view of environmental variables at global scales, including: sea-surface temperature, reflectance of light at various wavebands (remote-sensing reflectance, *R_{rs}*), and the photosynthetically-available radiation (visible light) incident on the sea surface [22]. However, the signals observed by satellites are from the sea surface and thus are blind to changes in the physical and biological properties of the ocean beneath the first few tens of metres [23]. To obtain a three-dimensional view of the ocean environment, Argo floats and ocean gliders equipped with sensors of temperature, salinity, and pressure (which determines depth) can be used to provide information on the vertical structure of the water column [24].

The biogeography of *Prochlorococcus* has been shown to be strongly related to environmental gradients of temperature and light, and inversely correlated to the presence of other phytoplankton groups indicated by the chlorophyll concentration [15,21,25,26]. As *Prochlorococcus* is the dominant phytoplankton in large areas of the world's oceans, it is important to be able to predict how its abundance might vary temporally and spatially in response to environmental and climate changes, and to assess seasonal and long-term changes in their biogeochemical cycles, trophic interactions and energy flow in oceanic food webs. To date, estimates of the global standing stock of *Prochlorococcus* [21] and its distribution in the world's oceans [20] do not take into account the vertical structure of cell abundance, which is an important feature of their biogeography and tightly coupled with resource gradients (e.g., light and nutrient concentrations) that govern their growth. Ignoring spatio-temporal changes in vertical structure could not only lead to potential errors in their contribution to water-column standing stocks but also hinder our ability to examine the impact of water-column stratification on the vertical partitioning of *Prochlorococcus* populations. Here, we present an empirical model that exploits two ocean-observing systems (Aqua-MODIS and Argo) to estimate the vertical and horizontal distribution of *Prochlorococcus* in the Atlantic basin. This approach captures both seasonal and interannual variations in the vertical distribution of *Prochlorococcus* cells, thus providing a powerful tool to examine the large-scale dynamics of standing stocks and their contribution to the marine organic carbon cycle.

2. Materials and Methods

The *Prochlorococcus* abundance model estimates the distribution of cells from the surface to the base of the photic zone using information on light penetration in the water column. The vertical distribution of *Prochlorococcus* has a form similar to the typical profile of primary production, which is determined by light availability and the photosynthetic response of phytoplankton to available light. Recognizing that primary production may indeed have a role in determining the vertical distribution of this genus in the ocean, we have used equations analogous to that of a photosynthesis-irradiance curve [27] to describe the relationship between cell abundance and the percentage of surface irradiance available at each depth z , henceforth referred to as the fractional PAR ($fPAR(z)$).

Although many subpopulations adapted to different light levels can coexist [25], the model is based on the assumption that there are two distinct populations of *Prochlorococcus* with distinct photophysologies: *ProI*, which dominates under high-light conditions found near the sea surface, and *ProII*, which has a preference for low-light conditions near the deep chlorophyll maximum (DCM). Vertical profiles of *ProI* and *ProII* are estimated from $fPAR(z)$. When these two populations are added, the resulting vertical profile of total *Prochlorococcus* cells, $Pro_{total}(z)$, peaks above the depth of the DCM (Z_{DCM}).

The series of equations used to estimate the vertical distribution of *Prochlorococcus* cells relies on information on four parameters that define the magnitude of the vertical profile of cell abundance: *Prochlorococcus* abundance at the sea surface (Pro_{surf}) and at the deep maximum (Pro_{max}), used to calculate *ProI* and *ProII*, respectively; the attenuation coefficient for PAR (K_dPAR), used to calculate $fPAR$ at each depth; and the depth of the deep chlorophyll maximum Z_{DCM} , used in the calculation of Pro_{max} . To estimate these four parameters, we explored their empirical relationships with environmental predictors that can be obtained from ocean observables or estimated using geo-location and time of the year.

2.1. Model Parameterization

Environmental variables that were related to K_dPAR , Z_{DCM} , and the growth of *Prochlorococcus* cells (Pro_{surf} and Pro_{max}) include: sea surface temperature (SST), remote-sensing reflectance at 443 ($R_{rs}(443)$) and 488 ($R_{rs}(488)$) nm, the photosynthetically-available radiation (PAR), the temperature at 200 m estimated from the Argo array (T_{200}), the solar zenith angle at noon (θ_s), and the day length (DL). The selection of these variables took into consideration some factors known to determine the distribution of this marine cyanobacterium. For example, *Prochlorococcus* is restricted to warm waters [13,16,20]; therefore, a thermal threshold was used. Additionally, the difference between SST and T_{200} is here used as a proxy for ocean stratification [28]. Remote-sensing reflectance of solar radiation in the visible domain is inversely related to light absorption by phytoplankton pigments and other light-absorbing substances, such that $R_{rs}(443)$ and $R_{rs}(488)$ are closely related to the concentration of chlorophyll at the sea surface. Therefore, the correlation between $R_{rs}(443)$ and Z_{DCM} is relatively strong, as Z_{DCM} tends to be deeper when there is less chlorophyll at the sea surface [29].

The sea-surface reflectance at blue wavelengths typically increases as the pigment biomass of most phytoplankton decreases (thus reducing light absorption). When the abundance of only *Prochlorococcus* cells is plotted against $R_{rs}(488)$ (sr^{-1}), we see that R_{rs} decreases with an increase in cell abundance, but after a certain threshold is reached, further decrease in R_{rs} is independent of the abundance of *Prochlorococcus*, suggesting phytoplankton other than *Prochlorococcus* might be determining changes in R_{rs} below this threshold (Figure S8b). The underwater light field is determined by K_dPAR in the model, which directly influences Z_{DCM} and the vertical distribution of *Prochlorococcus* cells. Light availability in the water column is also a function of the DL, which governs the daily integrated irradiance at the sea surface, and θ_s , which dictates the path length of light per unit of vertical distance within the water column (i.e., lower θ_s lead to lower light attenuation and a more vertical light path, with light reaching deeper waters). In addition, there is the influence of atmospheric components like aerosols and cloud

cover, which limit the incidence of PAR increasing the relative influence of inherent optical properties on the diffusion of light in the water column (i.e., equatorial upwelling regions).

Multilinear relationships between each parameter (K_dPAR , Z_{DCM} , Pro_{surf} , and Pro_{max}) and the abovementioned environmental variables were examined in a dataset from 13 Atlantic Meridional Transect (AMT) cruises (AMT 12–24) (Figure 1, Table S1) consisting of 704 vertical profiles (8722 observations) which covered a broad area of the Atlantic Ocean. For each cruise, vertical profiles of temperature, chlorophyll fluorescence, and downwelling PAR (British Oceanographic Data Centre—BODC) were measured alongside *Prochlorococcus* cell counts determined by flow cytometry. Details of the flow-cytometric analysis, the calculation of in situ variables (K_dPAR' and Z_{DCM}' , where the prime denotes in situ data), and programming languages and packages used for all calculations and data management are described in the *Suppl. Material*. Remote-sensing reflectance data were acquired from matching 8-day composites satellite imagery (Aqua-MODIS) [22].

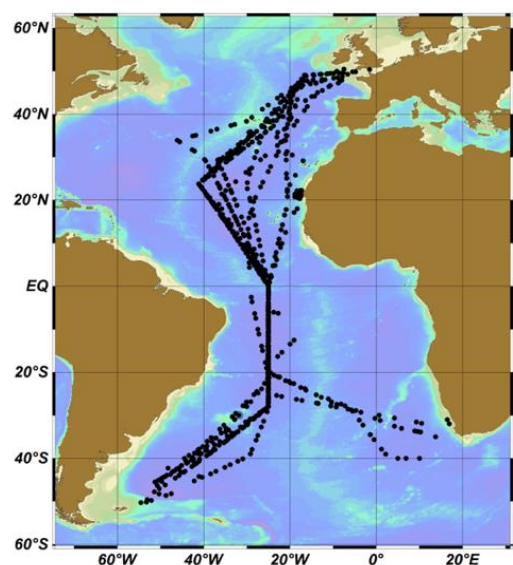


Figure 1. Transects of the 13 AMT cruises (704 stations) used to create the empirical model to predict the abundance of *Prochlorococcus* cells.

2.2. *Prochlorococcus* Abundance Predicted Using Ocean Observables

K_dPAR , Z_{DCM} , Pro_{surf} , and Pro_{max} were estimated based on their empirical relationships with six environmental variables: SST , $R_{rs}(443)$, $R_{rs}(488)$, T_{200} , DL , and θ_s . SST , $R_{rs}(443)$ and $R_{rs}(488)$ were acquired by the satellite Aqua-MODIS and provided by the NASA Ocean Color group [22]. Monthly climatological data of T_{200} [24] was extracted from Argo vertical temperature profiles. Satellite and Argo data products were regridded to a 4×4 km resolution, and every grid cell was used as input data for the *Prochlorococcus* cell abundance model.

Based on a subset of AMT cruises (Table S2), henceforth called *subdataset*, a group of variables was selected to predict each parameter using a backward stepwise multilinear regression [30]. The *subdataset* was randomly resampled allowing repetition of random data to generate the same number of observations as the original *subdataset* (Monte Carlo test with 2000 bootstrap permutations). In each *subdataset*, the multilinear relationship between the response and the selected explanatory variables was assessed and algorithm coefficients were computed [31]. The mean of each coefficient distribution was used in our predictive algorithms. Other variables were initially included such as mixed-layer depth, stratification index ($SST - T_{200}$) [28], and the downwelling irradiance (PAR) at the sea surface. These variables were excluded, both using the backward stepwise selection method and using the Akaike Information Criteria (AIC) to select the equation with the best fit to the response variable.

The work flow of all calculations, from satellite input variables, through to derived input variables, and to the final product of *Prochlorococcus* cell abundance integrated in the water column is displayed in Figure 2, with variables and their acronyms or symbols listed in Table 1.

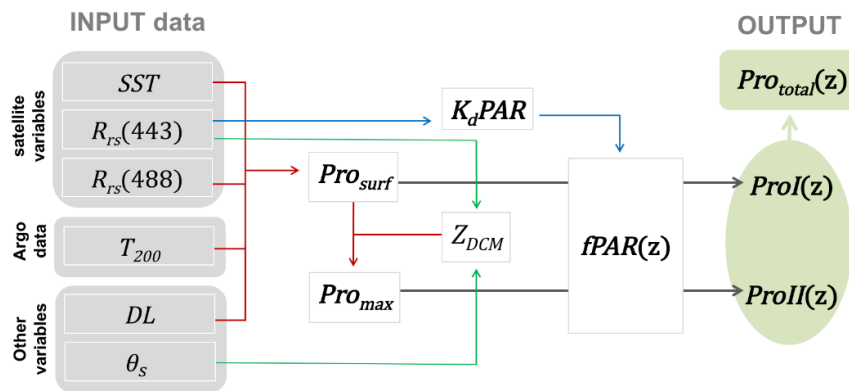


Figure 2. Flowchart of computations used to calculate the cell abundance of *Prochlorococcus*. Variable acronyms and symbols are described in Table 1.

Table 1. List of acronyms and symbols used in this manuscript (input variables used in the predictive model of *Prochlorococcus* cell abundance).

Symbol	Variable	Units	Source
SST	Sea surface temperature	°C	a
Rrs(443)	Remote-sensing reflectance at 443 nm	sr ⁻¹	a
Rrs(488)	Remote-sensing reflectance at 488 nm	sr ⁻¹	a
T ₂₀₀	Temperature at the depth of 200 m	°C	b
DL	Day length	hours	c
θ _s	Solar zenith angle at noon	degrees	d
K _d PAR	Calculated attenuation coefficient for the photo-synthetically available radiation	m ⁻¹	f
K _d PAR'	Measured attenuation coefficient for the photo-synthetically available radiation	m ⁻¹	e
DCM	Deep chlorophyll maximum		
DPM	Deep <i>Prochlorococcus</i> maximum		
Z _{DCM}	Calculated depth of the deep chlorophyll maximum	metres	f
Z _{DCM} '	<i>In situ</i> depth of the deep chlorophyll maximum	metres	f
fPAR(z)	Fractional PAR (proportion of surface PAR) at depth z	%	f
Pro _{surf}	Calculated <i>Prochlorococcus</i> cell abundance at the surface	cells mL ⁻¹	f
Pro _{surf} '	<i>In situ Prochlorococcus</i> cell abundance at the surface	cells mL ⁻¹	f
Pro _{max}	<i>Prochlorococcus</i> cell abundance at the DPM	cells mL ⁻¹	f
ProI	Calculated cell abundance of <i>Prochlorococcus</i> distributed over depth near the surface	cells mL ⁻¹	f
ProII	Calculated cell abundance of <i>Prochlorococcus</i> distributed over depth near the DPM	cells mL ⁻¹	f
Pro _{total} (z)	Calculated total <i>Prochlorococcus</i> cell abundance distributed over depth	cells mL ⁻¹	f
Pro _{int}	Calculated cell abundance of <i>Prochlorococcus</i> integrated in the surface 200 m of the water column	cells m ⁻²	f

a. Aqua-MODIS, Ocean Color, NASA (2014) [22]; b. Argo dataset (<http://argo.jcommops.org>); c. Forsythe et al. (1995) [32]; d. Cooper (1969) [33]; e. Kirk (2011) [9]; f. This work.

K_dPAR was estimated from satellite data using Equation (1):

$$K_dPAR = 0.0776 - 3.1673 R_{rs}(443) \quad (1)$$

derived from the correlation between in situ K_dPAR (K_dPAR') and $R_{rs}(443)$ ($r^2 = 0.75$). Then, K_dPAR was used to calculate the fractional PAR at depth ($fPAR(z)$) [9]. More details on the calculations to estimate K_dPAR are described in the *Suppl. Material*.

The two subpopulations of *Prochlorococcus*, *ProI* and *ProII*, are expressed as a function of the fractional PAR ($fPAR$) (Figure 3). $ProI(fPAR)$ is estimated based on the assumptions that these cells can be sustained at high concentrations if $fPAR \geq 1\%$ (0.01) and that this subpopulation represents cells adapted to high light, with an $E_k = 2.5\%$ (where E_k is the light saturation index).

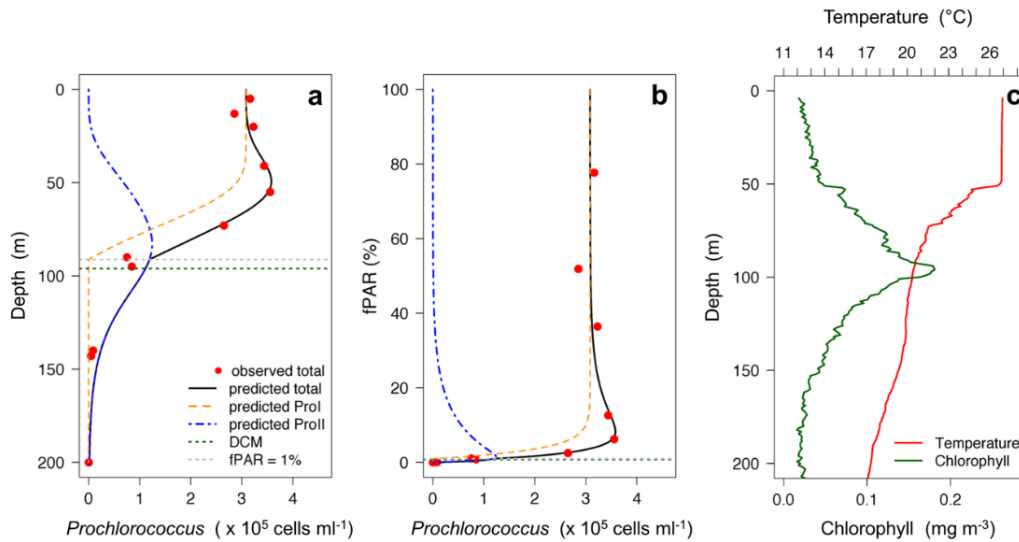


Figure 3. Vertical profiles of observed and estimated *Prochlorococcus* cell abundances (a) over depth and (b) over the fractional PAR $fPAR$, with (c) corresponding profiles of temperature and chlorophyll from CTD measurements at a site inside the North Atlantic Gyre (26° N, 50° W). For (a,b), in situ observations are represented by red dots, predicted profiles of *ProI* by the orange dashed line, predicted profiles of *ProII* by the blue dashed line, and predicted profiles of total *Prochlorococcus* abundance by the solid black line. Data from AMT 24 (2014).

$ProI(fPAR)$ was calculated using Equation (2):

$$ProI(fPAR) = Pro_{surf} \left[1 - \exp\left(-\frac{fPAR(z) - 0.01}{0.025}\right) \right] \quad (2)$$

with $ProI(fPAR) = 0$ if $fPAR \leq 0.01$ (1%). Photoinhibition of cell accumulation (i.e., the negative slope of the PE curve described in Platt et al. (1980) [27]) is not exhibited by this subpopulation, thus the maximum cell concentration of $ProI(fPAR)$ is equal to the concentration of *Prochlorococcus* cells at the high light intensities found at the sea surface (Pro_{surf}). Pro_{surf} is calculated using Equations (3)–(5):

$$Pro_{surf} = n_0 [a_3 SST + b_3 R_{rs}(488) + c_3 DL + d_3 T_{200} + e_3 (SST \times R_{rs}(488))], \quad (3)$$

$$n_1 = 1 - \left(\frac{17 - SST}{17 - 13} \right), \quad (4)$$

and

$$n_2 = 1 - \left(\frac{0.004 - R_{rs}(488)}{0.004 - 0.001} \right) \quad (5)$$

where a_3 , b_3 , c_3 , d_3 , and e_3 are empirical coefficients listed in Table 2, $n_0 = n_1$ if $SST < 17^\circ$ C, $n_0 = n_2$ if $R_{rs}(488) < 0.004$ sr $^{-1}$ and $SST - T_{200} < 10^\circ$ C, and $n_0 = 1$ otherwise. The model assumes that *Prochlorococcus* is restricted to warm waters [13,34], thus cell abundance progressively decreases as sea surface temperatures (SST) fall below 17° C and become absent where SST is less than 13° C

(Equation (4)) (Figure S8a). The model also adopts the widely-held view that *Prochlorococcus* cells are absent in productive waters with high surface chlorophyll concentrations (thus low remote-sensing reflectance (Equation (5))), which is shown by the gradual decrease in cell abundance once $R_{rs}(488)$ is lower than 0.004 (Figure S8b). The day length (DL) was calculated according to Forsythe et al. (1995) [32].

To estimate the abundance of $ProII(fPAR)$, a photoinhibition component was included (Equation (6)):

$$ProII(fPAR) = Pro_{max} \left[1 - \exp\left(-\frac{fPAR(z)}{0.005}\right) \right] \exp\left(-\frac{fPAR(z)}{0.1}\right). \quad (6)$$

Table 2. Parameters and coefficients used in Equations (1) to (8) with their standard deviations (σ).

Output	Input (s)	Equation	Parameter	Parameter Value	Parameter σ
K_dPAR		(1)	intercept	0.776×10^{-1}	0.020×10^{-1}
	$R_{rs}(443)$	(1)	slope	-3.1673×10^0	0.195×10^0
Z_{DCM}		(8)	intercept	1.241×10^1	0.786×10^1
	$R_{rs}(443)$	(8)	slope ₁	1.021×10^4	0.066×10^4
	θ_s	(8)	slope ₂	2.227×10^{-1}	2.381×10^{-1}
Pro_{surf}	SST	(3)–(5)	a_3	3.254×10^4	0.030×10^4
	$R_{rs}(488)$	(3)–(5)	b_3	9.762×10^7	0.104×10^7
	DL	(3)–(5)	c_3	-2.080×10^4	0.043×10^4
	T_{200}	(3)–(5)	d_3	-2.117×10^4	0.029×10^4
	$SST, R_{rs}(488)$	(3)–(5)	e_3	-4.421×10^6	0.041×10^6
Pro_{max}		(7)	a_7	-1.153×10^5	0.194×10^5
	Z_{DCM}	(7)	b_7	1.837×10^3	0.014×10^3
	Pro_{surf}	(7)	c_7	2.951×10^{-1}	0.087×10^{-1}

$ProII(fPAR)$ cells are adapted to lower light intensities ($E_k = 1\%$), reaching a subsurface maximum cell concentration represented by Pro_{max} , which in turn was calculated using Equation (7):

$$Pro_{max} = a_7 + b_7 Z_{DCM} + c_7 Pro_{surf} \quad (7)$$

where Z_{DCM} is the depth of the deep chlorophyll maximum, and a_7 , b_7 , and c_7 are coefficients listed in Table 2. The DCM depth, Z_{DCM} , was determined using Equation (8):

$$Z_{DCM} = 12.41 + 10210 R_{rs}(443) - 0.2227 \theta_s \quad (8)$$

where θ_s is the absolute solar zenith angle at noon (degrees). Equation (8) was derived from the multilinear relationship between observed Z_{DCM} (Z_{DCM}'), $R_{rs}(443)$ and the solar zenith angle at noon (θ_s) in selected cruises ($r^2 = 0.73$) (Figure 4).

The absolute solar zenith angle at noon θ_s was derived from the sun declination [33], as detailed in the *Suppl. Material*.

After computing the depth z (in metres) associated with a particular $fPAR$ [9], the total *Prochlorococcus* cell abundance at any depth z ($Pro_{total}(z)$) was determined as the sum of $ProI(z)$ and $ProII(z)$ in Equation (9):

$$Pro_{int}(z) = ProI(z) + ProII(z) \quad (9)$$

and then integrated over the top 200 m of the water column (Pro_{int}) using Equation (10):

$$Pro_{int} = \int_{z=0}^{z=200} Pro_{total}(z) dz. \quad (10)$$

Mean coefficients in the model equations and their standard deviations (σ) are listed in Table 2. Examples of *Prochlorococcus* cell abundance profiles ($Pro_{total}(z)$) observed in situ and predicted by the model within the North and South Atlantic Gyres and in the gyre periphery (areas outside the gyre limits and also outside the ECZ, where SST < 25 °C but *Prochlorococcus* cells are still abundant) are shown in Figure S7.

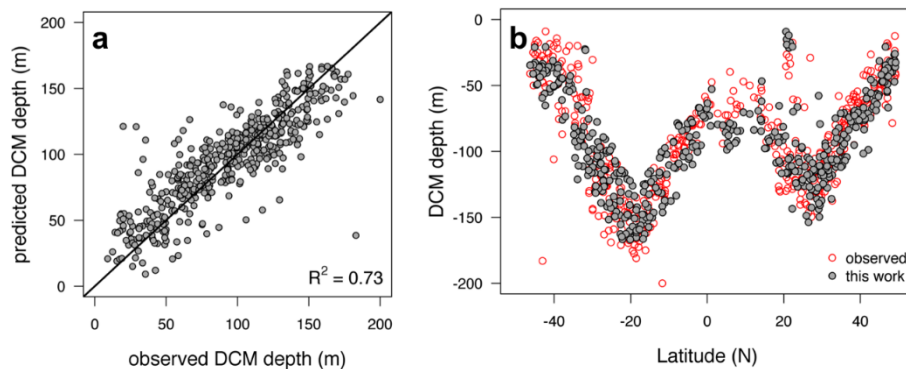


Figure 4. (a) Comparison between observed versus predicted depth of the deep chlorophyll maximum (Z_{DCM}) across the Atlantic Ocean (locations displayed in Figure 1) using Equation (8) of the present work; (b) Observed (AMT12-24, $n = 693$ observations) and predicted Z_{DCM} ($n = 449$) in the Atlantic Ocean (AMTs 12 to 24, locations displayed in Figure 1). For each CTD cast, observed Z_{DCM} was determined as the depth of the maximum chlorophyll concentration measured using the CTD fluorometer.

3. Results

3.1. Two-Component Model Validation

The derived parameters of the model (Z_{DCM} , K_d^{PAR} , Pro_{surf} , Pro_{max}) that describe the shape of the abundance profile and the final products $Pro_{total}(z)$ and Pro_{int} were validated using 13 AMT cruises, which cover a broad swath of the Atlantic basin, and data from BATS (Bermuda Atlantic Time-Series Study).

Model estimates were compared with in situ observations using the approach proposed by Brewin et al. (2015) [31], which includes four statistical metrics: root mean square error (Ψ); average bias (δ); centre-pattern (or unbiased) root mean square error (Δ); and the adjusted coefficient of determination (r^2). For this, we assumed variables present a normal frequency distribution in the natural environment. Results of the statistical tests are summarised in Table 3.

When using in situ observations of the derived parameters as inputs for the model, particularly Pro_{surf} and Z_{DCM} (in which case Equations (1), (3)–(5) and (10) are excluded), our model robustly predicts the vertical distribution of *Prochlorococcus* cells in the water column (i.e., $Pro_{total}(z)$, $r^2 = 0.84$, Figure 5b) and, consequently, produces reasonable estimates of cell concentrations integrated in the top 200 m of the water column (i.e., Pro_{int} , $r^2 = 0.85$, Figure 6). However, when using remotely-sensed environmental variables as inputs to estimate the derived parameters (full model from remote-sensing data), the predictive skill of the model to $Pro_{total}(z)$ and Pro_{int} decreases to $r^2 = 0.58$ and $r^2 = 0.48$, respectively (Table 3; Figures 5c and 7a,b). This increase in error is primarily caused by the difficulty in estimating Pro_{surf} from satellite ($r^2 = 0.50$ Figures 7c,d and S9b). The reduction in performance may also be attributed to the nature of comparing observations at vastly different spatial and temporal scales: in situ cell abundance counts were taken in a few millilitres of seawater at a determined time point where environmental conditions can change in hours or days, whereas satellite data were extracted from 8-day composites and pixels cover an area of 16 km² and Argo data were extracted from a climatology (monthly average over 6 years). Overall, the satellite-derived model is negatively biased ($\delta = -0.572 \times 10^{12}$ cells cm⁻²), and tends to underestimate cell concentrations at most depths

(Figure 5c). However, the spatial variability of integrated cell abundance is still well represented (Figure 7b).

Table 3. Response variables with their respective root mean square error (Ψ), bias (δ), centre-root (unbiased) mean square error (Δ), and determination coefficient (r^2) when compared with in situ data from 13 AMT cruises. Variable definitions are listed in Table 1.

Variable	Equation	Ψ	δ	Δ	r^2
K_dPAR	(1)	5.136×10^{-3}	-0.321×10^{-3}	0.512×10^{-3}	0.75
Z_{DCM}	(8)	2.084×10^1	-0.101×10^1	2.081×10^1	0.73
Pro_{max}^1	(7)	5.872×10^4	-0.054×10^4	5.872×10^4	0.44
$Pro_{total}(z)^1$	(9)	3.775×10^4	-0.361×10^4	3.758×10^4	0.84
Pro_{int}^1	(10)	3.682×10^{12}	-1.047×10^{12}	3.529×10^{12}	0.85
Pro_{max}^2	(7)	5.805×10^4	-0.349×10^4	5.794×10^4	0.40
$Pro_{total}(z)^2$	(9)	4.038×10^4	-0.479×10^4	4.010×10^4	0.82
Pro_{int}^2	(10)	4.146×10^{12}	-1.214×10^{12}	3.964×10^{12}	0.81
Pro_{surf}^3	(3)–(5)	6.551×10^4	1.237×10^4	6.434×10^4	0.50
Pro_{max}^3	(7)	6.210×10^4	0.297×10^4	6.203×10^4	0.32
$Pro_{total}(z)^3$	(9)	6.176×10^4	0.466×10^4	6.159×10^4	0.58
Pro_{int}^3	(10)	6.651×10^{12}	-0.572×10^{12}	6.651×10^{12}	0.48

Prochlorococcus cell abundances calculated using: ¹ in situ Pro_{surf} (Pro_{surf}) and in situ Z_{DCM} (Z_{DCM}); ² in situ Pro_{surf} and modelled Z_{DCM} ; ³ modelled Pro_{surf} and modelled Z_{DCM} .

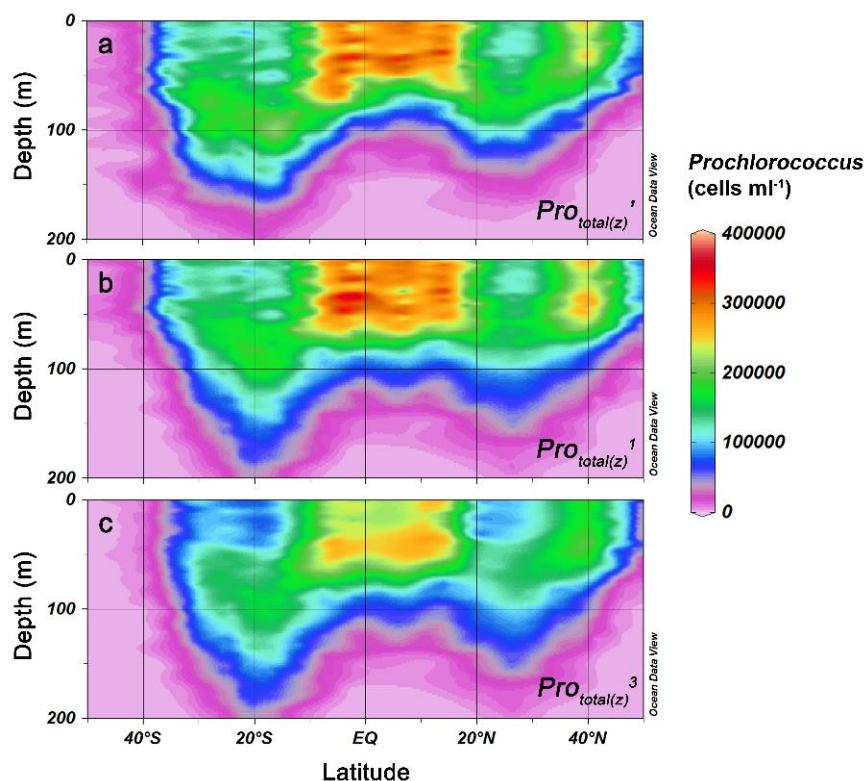


Figure 5. Vertical profiles of *Prochlorococcus* cell abundance over depth ($Pro_{total}(z)$) across the Atlantic Ocean (locations displayed in Figure 1): (a) observed in situ on AMTs 12–24 ($Pro_{total}(z)$); (b) predicted using the partial model with observed inputs of Pro_{surf} and Z_{DCM} ($Pro_{total}(z)^1$ from Equations (1) to (2) and (6) to (7)); and (c) predicted using the full model with remote-sensing inputs ($Pro_{total}(z)^3$ from Equations (1)–(9)).

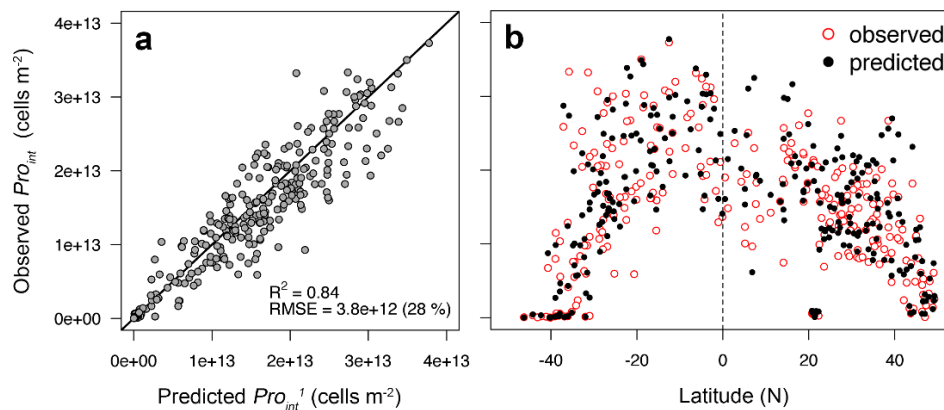


Figure 6. (a) Comparison between observed and predicted *Prochlorococcus* cell abundance integrated in the water column (Pro_{int}^1) across the Atlantic Ocean (locations displayed in Figure 1) using the partial model where in situ observations of Z_{DCM} , K_dPAR , and Pro_{surf} are used as inputs (i.e., Equations (1), (3)–(5), and (8) are excluded); (b) Observed and predicted Pro_{int}^1 across the Atlantic Ocean (AMTs 12–24).

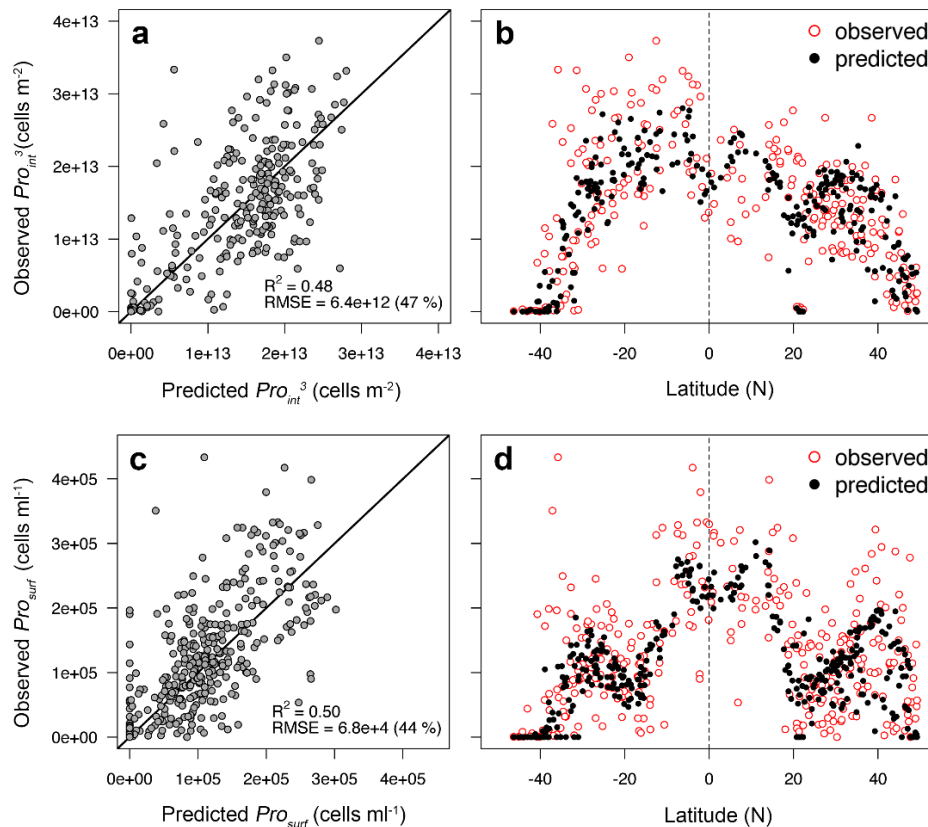


Figure 7. (a) Comparison between observed and predicted *Prochlorococcus* cell abundance integrated in the water column (Pro_{int}^3) across the Atlantic Ocean (locations displayed in Figure 1) using the complete model (Equations (1)–(10) of the present work); (b) Observed and predicted Pro_{int}^3 across the Atlantic Ocean (AMTs 12–24); (c) Comparison between observed and predicted *Prochlorococcus* cell abundance at the sea surface (Pro_{surf}) using Equations (3)–(5) of the present work; (d) Observed and predicted Pro_{surf} across the Atlantic Ocean (AMTs 12–24).

3.2. Two-Component Model Output

In the present work, we opt for using a two-component model (*ProI* + *ProII*) that is able to determine the maximum abundance of *Prochlorococcus* cells when it occurs at depth (Figure S7). The relevance of this deep component *ProII* to determine the vertical distribution of *Prochlorococcus* cells was tested by comparing two-component model output with a model that has only the component *ProI*. Details of this comparison are described in the *Suppl. Material*.

According to estimates of the two-component model, the Atlantic basin hosts 7.4×10^{26} *Prochlorococcus* cells (32 Mt of carbon, assuming an intracellular carbon concentration of $50 \text{ fg C cell}^{-1}$ [19]), concentrated mainly in warm stratified waters. When combined, subtropical gyres hold the largest cell concentrations (35%), followed by the area near the Equatorial Convergence Zone (ECZ) which carries 30% of the Atlantic cell stock (Table 4, Figure 8). The total standing stock in the two Atlantic subtropical gyres varies according to both their areal extent, which expands and contracts seasonally (Figures 8 and 9a,b), and to their euphotic depth (Figure 9c,d), which governs the vertical distribution of cells and the depth range over which they occur. Subtropical gyres were determined as areas where the concentration of chlorophyll at the sea surface is lower than or equal to 0.075 mg m^{-3} [35] (more information in the *Suppl. Material*).

Table 4. Predicted *Prochlorococcus* standing stock in the oceans, integrated horizontally and vertically at each area. Values were computed using Equations (1)–(10), with monthly climatology products used as input variables [22], then averaged over the year. Pro_{int}^3 , Pro_{surf}^3 and Pro_{max}^3 were calculated at specific geographic locations within each Atlantic gyre (coordinates in the table).

	Standing Stock (Cells)	Total Carbon * (Megatonnes C)	Pro_{int}^3 (Cells m^{-2})	Pro_{surf}^3 (Cells mL^{-1})	Pro_{max}^3 (Cells mL^{-1})
Global	3.4×10^{27}	171			
Atlantic Ocean	7.4×10^{26}	37			
Equatorial Convergence Zone	2.2×10^{26}	11			
ECZ: 2°S, 22°W			1.7×10^{13}	2.2×10^5	0.7×10^5
North Atlantic Gyre	1.0×10^{26}	5.1			
NAG: 26° N, 50° W			1.6×10^{13}	0.7×10^5	1.3×10^5
South Atlantic Gyre	1.6×10^{26}	8.2			
SAG: 20° S, 20° W			2.2×10^{13}	1.0×10^5	1.7×10^5

* using $50 \text{ fg C cell}^{-1}$ to convert cell concentrations to carbon units [19].

To better visualise the seasonal dynamics of these two factors controlling the standing stock of *Prochlorococcus*, we assessed both of these ocean properties for the North and South Atlantic Gyres, hitherto referred to as the NAG and the SAG. In their respective summer months, both the northern and southern gyres expand (Figure 9a,b) as the sea surface temperature (Figure 9e,f) and the intensity of the incident irradiance (*PAR*) increase [7]. The increase in these two factors foster stratification of the water column that both reduces the supply of nutrients from depth and increases the average light intensity to which phytoplankton cells are exposed [9]. The high incident irradiance leads to a reduction in the concentration of *Prochlorococcus* cells at surface (Pro_{surf}) (Figure 9g,h), but since the light penetrates deeper in the water column, the growth of *Prochlorococcus* cells close to the DCM (Pro_{max}) is enhanced and higher concentrations are found at the DCM than at the sea surface (Figure 9i,j). Thus, the vertical profiles of cell abundance vary over the annual cycle, with Pro_{max} reaching highest concentrations from spring to autumn (Figures 8 and 9i,j), whereas Pro_{surf} is highest during winter (Figures 8 and 9g,h). The integrated cell abundance in the water column (Pro_{int}) is influenced by the depth of the euphotic layer and Pro_{max} , showing seasonal variability that resembles that of Pro_{max} and thus is inverse to Pro_{surf} (Figure 9k,l). The resemblance between Pro_{int} and Pro_{max} was also observed in their interannual variability in both gyres (Figure 10c,d,i,j).

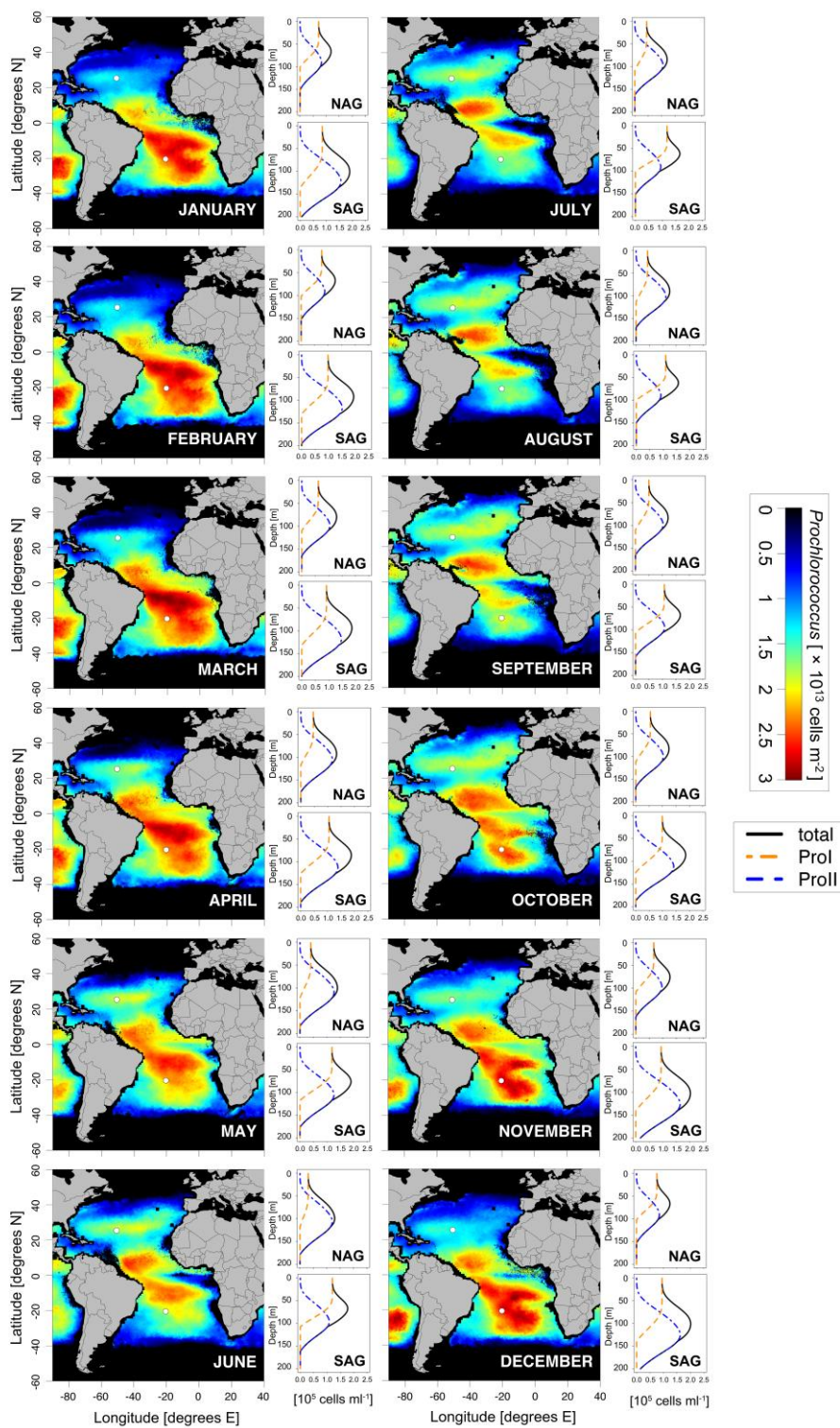


Figure 8. Estimated monthly distribution of the *Prochlorococcus* cells integrated in the top 200 m of the water column (Pro_{int}) (cells m^{-2}), with correspondent vertical profiles of estimated *Prochlorococcus* cell abundance (cells l^{-1}) at sites (white dots) in the North Atlantic Gyre (NAG) and South Atlantic Gyre: $Prol(z)$ is indicated by the orange dashed line, $Proll(z)$ by the blue dashed line, and the total *Prochlorococcus* abundance by the solid black line. Cell abundance was calculated based on the monthly climatology of environmental variables [22].

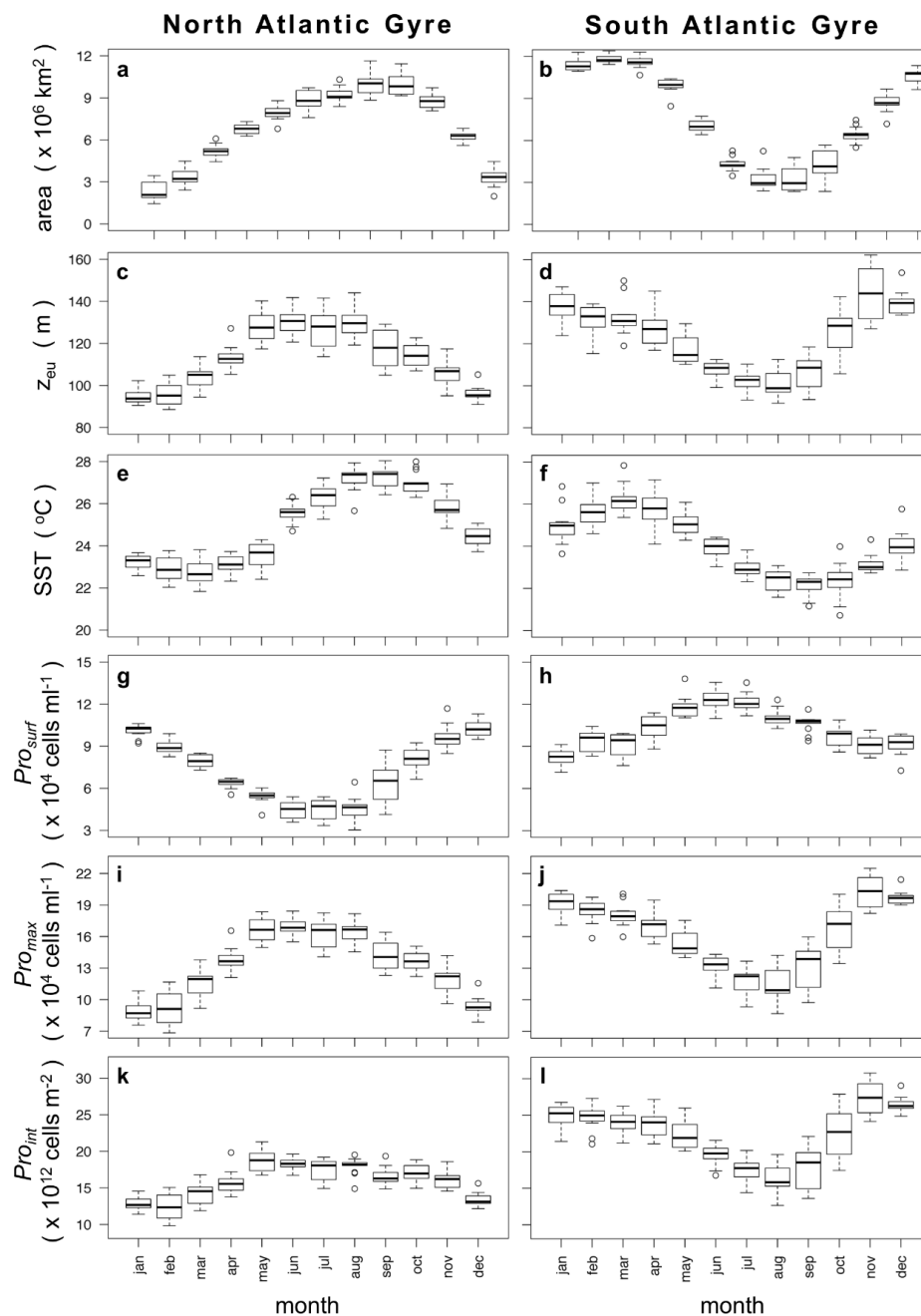


Figure 9. Monthly averages of (a) the areal extent of the North Atlantic Gyre (NAG) and (b) South Atlantic Gyre (SAG); (c) the euphotic depth z_{eu} at the NAG and (d) the SAG; (e) sea surface temperature SST at the NAG and (f) the SAG; (g) the estimated *Prochlorococcus* cell abundance at the sea surface (Pro_{surf}) at the NAG and (h) the SAG; (i) *Prochlorococcus* cell abundance at the deep maximum (Pro_{max}) at the NAG and (j) the SAG; and (k) *Prochlorococcus* cell abundance integrated in the water column (Pro_{int}) at the NAG and (l) the SAG. Subtropical Gyres were defined as regions where the surface chlorophyll concentrations were lower than 0.075 mg m^{-3} . The euphotic depth was estimated using the calculated K_dPAR using Equation (1), and SST measurements were taken from monthly satellite composites from January 2003 to December 2014 [22]. *Prochlorococcus* cell abundance was computed using monthly averaged input variables for the years 2003–2014 [22], at specific locations inside the Atlantic gyres: NAG: 26° N , 50° W ; SAG: 20° S , 20° W .

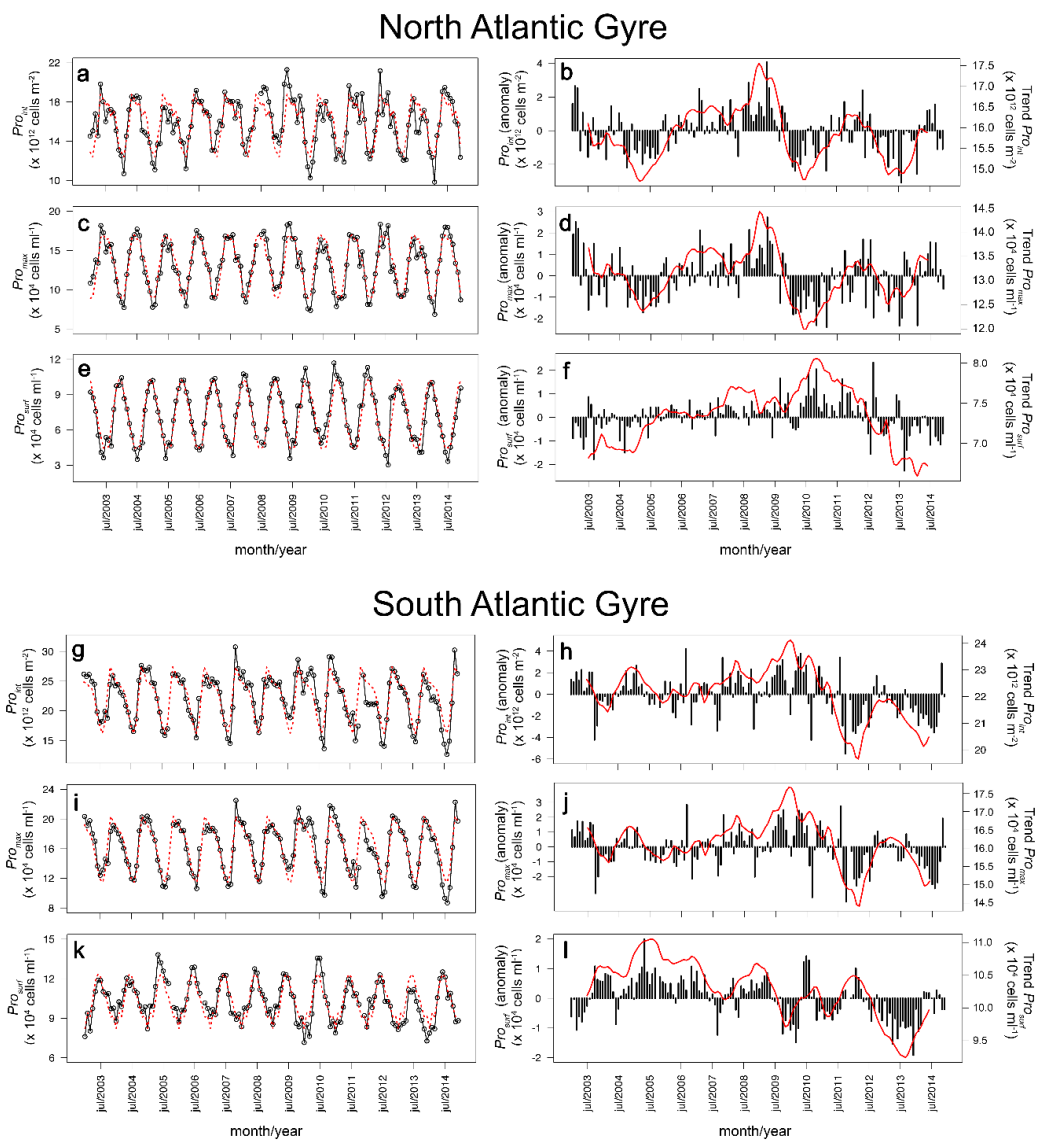


Figure 10. Time series of (a,g) the estimated *Prochlorococcus* cell abundance integrated in the water column (Pro_{int}), (c,i) estimated *Prochlorococcus* cell abundance at the deep maximum (Pro_{max}), and (e,k) estimated *Prochlorococcus* cell abundance at surface (Pro_{surf}), at one location (26° N, 50° W) in the North Atlantic Gyre (NAG) (a–f), and one location (20° S, 20° W) in the South Atlantic Gyre (SAG) (g–l). Figures (b,d,f,h,j,l) show the time-series anomalies (black bars) and trends (red lines). Anomalies were calculated by subtracting the monthly climatology (dashed red lines in figures (a,c,e,g,i,k)) from the calculated values for each month (black lines in figures (a,c,e,g,i,k)).

In general, the standing stock of *Prochlorococcus* cells integrated over the gyre area is 1.7 times higher in the South Atlantic Gyre (SAG) than in the North Atlantic Gyre (NAG) (Table 4), regardless of the season (Figure 9k,l). No clear long-term temporal changes of Pro_{int} and Pro_{max} were observed in either of the gyres (Figure 10a,b,g,h), although a mode shift (between positive and negative anomalies) of approximately 3–5 years was observed in the NAG (Figure 10a,b). Pro_{surf} decreased in the SAG (Figure 10k,l), whereas in the NAG there was an increase in cell abundance from 2002 to 2011, followed by a step decrease from 2012 to 2014 (Figure 10e,f), which could be associated with the degradation of MODIS R_{rs} signals that started in 2012.

4. Discussion

The two-component model successfully reproduces the vertical distribution of the cell abundance of *Prochlorococcus* across the Atlantic Basin, including the formation of a deep abundance maximum a few metres above the DCM (see Figure 3). When provided with in situ measurements of surface cell abundance (Pro_{surf}), the model accurately predicts the vertical distribution of cells ($r^2 = 0.83$, see Table 3), regardless of the geographic location, showing that physical and biological processes that take place in surface layers of the water column are tightly coupled to those that occur at depth. However, when satellite data are used to determine Pro_{surf} , model estimates of the integrated cell abundance in the water column (Pro_{int}) are more precise in the Atlantic Ocean than in other ocean basins (see Table 3), as the empirical relationships used in this algorithm were derived from data collected in the Atlantic.

Despite having roughly similar global estimates, the predicted global distribution patterns of *Prochlorococcus* cells are markedly different from previous studies, with our model showing higher surface cell concentrations in the area near the Equatorial Convergence Zone (ECZ) and on the periphery of subtropical gyres, and lower surface cell abundance in the core of the gyres. This distribution pattern is supported by in situ observations made in several transect cruises across the Atlantic Ocean [13,16] (see Figure 7d). Conversely, surface distributions of *Prochlorococcus* presented by Flombaum et al. (2013) [20] show higher cell concentrations not only in the ECZ, but also in the western sector of the ocean basins (which includes the central portion of the subtropical gyres) due to the strong relationship between *Prochlorococcus* cell abundance and water temperature, especially if observations at depth are taken into account.

Similar to the present study, Flombaum et al. (2013) [20] used a series of empirical equations that relate *Prochlorococcus* cell concentrations at the surface and at depth to the vertical structure in temperature and daily PAR. Thus, their model assumes that the same environmental factors that influence cell abundance at the surface also govern the variability in cell concentrations at depth. In the present model, the surface distribution of cells is primarily influenced by environmental conditions at the sea surface (except the variable T_{200} which is used as a proxy for stratification and hence nutrient input from depth). To estimate cell abundance at depth, we include an additional parameter: the maximum cell abundance at depth (Pro_{max}). The analysis of in situ data shows that the profile of *Prochlorococcus* is directly influenced by Pro_{max} , which in turn is related to the water-leaving radiance at 443 nm ($R_{rs}(443)$). Thus, Pro_{max} is highest when $R_{rs}(443)$ is highest (i.e., in optically clear waters, there is less phytoplankton pigment at the surface, therefore less light absorption, leading to an increase in water-leaving irradiance at blue wavelengths). Conversely, cell concentrations at the surface are inversely related to $R_{rs}(443)$ where sea surface temperatures are high (see coefficient e_3 in Table 2), which occurs in the interior of subtropical gyres. Partitioning our *Prochlorococcus* population into two components ($ProI$ near the surface and $ProII$ at depth) allowed us to include the deep peak in *Prochlorococcus* cell abundance that is routinely observed in subtropical waters [13,15,16,36] and which contributes significantly to the vertically integrated cell abundance, especially in periods when surface irradiance (PAR) is high or increasing over time (i.e., summer, spring). This deep abundance maximum is neglected in the previous models, which may explain why global cell stock in Flombaum et al. (2013) [20] is lower than that estimated in the present study. Additionally, instead of using PAR, our model uses $fPAR$ to determine the vertical distribution of cells. The reason for using a relative rather than absolute value of irradiance is because the shape of phytoplankton pigment and the abundance and productivity profiles in open ocean waters have been shown to follow changes in light attenuation rather than fluctuations in instantaneous light [37,38]. This happens possibly because PAR varies over a timescale of hours, whereas $fPAR$ reflects a longer-term (days or weeks) change in the availability of light at depth and how the microbial community (including phytoplanktonic pigmented cells) responds to these variations over longer time periods.

As a consequence of the differences in approach between the present study and those of Flombaum et al. (2013) [20], the seasonality and temporal variability of the global *Prochlorococcus* cell stock are markedly different between the two models. Our results show that global and regional cell

stocks of *Prochlorococcus* are relatively constant over time, not showing any discernible long-term trend over the 12-year study period (2003–2014). This is in part due to the areal extent of the gyres being relatively uniform from 2003 to 2014 (if seasonal oscillations are discarded), when estimated on the basis of satellite observations of chlorophyll concentration at the sea surface [7]. This result is also consistent with the view that the *Prochlorococcus* population consists of a “federation” of physiologically diverse cells that exhibits dynamic stability [34].

Our model detected a positive–negative anomaly cycle of 3–5 years, similar to that observed between 1991 and 2004 in the North Pacific Gyre near Hawaii (HOT time series) [15]. This cyclical oscillation may be associated with changes at depth, such as variations in the volume and/or vertical oscillations of subtropical mode waters (STMW). The STMW are voluminous subsurface (depths between ~150 and ~400 to 600 m in the Atlantic gyres) water masses located in the subtropical gyres, characterised by unique high temperature and salinity conditions that make this water mass vertically homogeneous [39]. Therefore, in subtropical gyres, oscillations in the STMW directly influence nutrient supply from depth to surface and, consequently, phytoplankton growth, including the growth of *Prochlorococcus*.

Water-column stability also varies seasonally, resulting in marked seasonal changes in the concentrations of *Prochlorococcus* cells. As ~57% of the global ocean’s area is located in the Southern Hemisphere [40], of which the occupation of subtropical gyres is greater than in the Northern Hemisphere (i.e., Figure 9a,b), the seasonal variability observed in the global *Prochlorococcus* cell stock (see Figure S6a) is mostly influenced by a combination of environmental conditions in the Southern Hemisphere, such as the areal extent of the Southern Subtropical Gyres (see Figure 9b), underwater light conditions, and vertical structure of the water column. As solar radiation levels increase during the summer, the gyres expand reaching the maximal extent, and the water column becomes warmer and more stratified in the gyre’s interior. This leads to extreme high-light and low-nutrient conditions that reduce the growth of phytoplankton at the surface [5]. High light levels at the sea surface also result in a reduction in the intracellular concentration of photosynthetic pigments as a consequence of phytoplankton photoacclimation [5], which is another factor leading to lower surface concentrations of chlorophyll at the sea surface in the summer [41].

The increased surface irradiance and reduced phytoplankton pigment concentration at the surface allow solar irradiance to penetrate deeper within the water column, and the lower intracellular pigment concentrations induced by higher irradiance lead to a decrease in K_dPAR and a consequent increase in the limits of the euphotic zone (see Figure 9c,d). Therefore, the depth range over which *Prochlorococcus* has enough light to achieve net growth extends deeper, resulting in higher integrated cell abundances during the summer (see Figure 9k,l). In contrast, during the winter, lower surface irradiances and increased mixing in the water column are accompanied by an increase in cellular chlorophyll concentrations at the sea surface, leading to the contraction of the gyre’s extension [41,42]. Previous assessments of seasonal variations in *Prochlorococcus* populations based on in situ observations show that, in the Atlantic subtropical gyres, standing stocks of *Prochlorococcus* are larger during spring when compared with autumn [16]. Conversely, at the periphery of the North Atlantic gyre, *Prochlorococcus* is most abundant during summer and autumn [14,43]. In the North Pacific Gyre (HOT station), Rabouille et al. (2007) [15] and Malmstrom et al. (2010) [14] reported no significant seasonal changes in the integrated abundance of *Prochlorococcus* in the euphotic layer, but a noticeable seasonal shift in their vertical distribution was observed.

Differences between *Prochlorococcus* cell stocks in the NAG and the SAG may be a consequence of physical processes that govern nutrient delivery in the gyres: the degree of water column stratification and the proximity of the STMW to the bottom of the photic zone. In the SAG, the water column is strongly stratified at the bottom of the mixed layer, and a shallow pycnocline is formed during spring when surface waters start to warm. The deep thermocline occurs at 80–120 m and coincides with the nutricline; above this depth horizon the water column is relatively homogeneous (see Figure S7i). However, the amount of total kinetic energy input at the surface is low, leading to low mixing [44]

within the surface ocean. The higher concentration of *Prochlorococcus* cells ($Pro_{int} = 2.2 \times 10^{13}$ cells m^{-2}) in the SAG when compared with the NAG may be a consequence of either a thinner underlying STMW in the SAG or the unique vertical structure of density of this STMW [39] that may influence nutrient input from depth to the euphotic layer. Conversely, the NAG has the thickest STMW in the global ocean, and the temperature at 200 m is considerably warmer (see Figure S7f) than that found in the SAG, the ECZ, or even the NAG periphery (see Figure S7c). The lower stratification combined with higher temperatures at depths between 100 and 200 m indicates an even deeper thermocline and nutricline, leading to a lower nutrient flux from depth and thereby resulting in the lower *Prochlorococcus* cell stocks in the NAG ($Pro_{int} = 1.6 \times 10^{13}$ cells m^{-2}).

Prochlorococcus numerically dominates vast expanses of the warm and strongly-stratified open ocean [13,15,34,45,46]. The sensitivity of the *Prochlorococcus* population as a whole to changes in physical forcing [12], such as decreased kinetic energy input to the water column, resulting in low turbulent mixing [44] and long-period internal oscillations in subsurface water masses that can lead to changes in nutrient supply from depth [39], makes this genus an ideal indicator of water-column dynamics. The preferred habitat of *Prochlorococcus*, the ocean's subtropical gyres, expands and contracts according to seasonal changes in stratification, leading to significant spatiotemporal changes in the standing stocks of *Prochlorococcus* cells. Additionally, variations in *Prochlorococcus* cell stocks are a consequence of the collective physiological response of this genetically diverse assemblage of cells to both abiotic (temperature, nutrients), and biotic factors (grazing pressure, viral infection, sinking), the latter of which were not explored in the present work. Nevertheless, our model is able to recreate the basin-scale patterns in the vertical distribution of *Prochlorococcus* cells, which is a crucial first step to quantify the role of this globally important cyanobacterium in marine biogeochemical cycles.

5. Conclusions

Despite their minute size and cellular biomass [47], *Prochlorococcus* represents a significant amount of global carbon biomass: 171 Mt C contained in $\sim 3.4 \times 10^{27}$ cells. Most of this biomass is concentrated in areas near the Equatorial Convergence Zone and in the subtropical gyres. In the Atlantic, no significant temporal change was observed over the period of 2003–2014, but marked seasonal variations in cell abundance occur inside the subtropical gyres, where cell abundances are highest in the spring and summer and lowest during the winter. Although the global estimate presented here is similar to that calculated in a previous model [20], the spatial and temporal patterns in the abundance of *Prochlorococcus* cells differ. Our results are in agreement with observations made in the natural environment [13,15,16,36] and provide an unprecedented three-dimensional view of the distribution of *Prochlorococcus* biomass in the Atlantic ocean using remote-sensing observations.

This depth-resolved empirical model helps advance our ability to examine temporal changes in the biomass of *Prochlorococcus* over basin scales. Although the model captures the light dependence of *Prochlorococcus* abundance, there is scope for further refinements. The parameterisation of the model is based on a dataset that is geographically biased to the Atlantic basin, whereas data from the Pacific and Indian Oceans (PANGAEA dataset after 2002) were used only for validation (see *Suppl. Material*). A broader coverage of spatial in situ data can improve the equation used to estimate the abundance of *Prochlorococcus* cells at the sea surface (Pro_{surf}) by regionally tuning it for each ocean basin. Improvement of estimates of Pro_{surf} will increase the model's ability to accurately predict of the vertical distribution of *Prochlorococcus* cells in other ocean basins.

Supplementary Materials: Additional information to this manuscript is available online at www.mdpi.com/2072-4292/10/6/847/S1.

Author Contributions: All authors contributed to the elaboration (writing) of this manuscript. Additionally, P.K.L., H.A.B., R.J.W.B. and S.S. conceived the model, G.A.T. and M.Z. provided flow cytometric data acquired on the cruises AMT 12 to 21, and G.D. provided and processed the Argo dataset.

Acknowledgments: This work was supported by the Atlantic Meridional Transect Program (AMT) and the Brazilian National Council for Scientific and Technological Development (CNPq) (PhD GDE scholarship 211546/2013-5). The AMT dataset is supported by the UK Natural Environment Research Council National Capability funding to Plymouth Marine Laboratory and the National Oceanography Centre, Southampton. The authors would like to thank the British Oceanographic Data Centre (BODC), and the International Argo Program and national programs that contribute to it (<http://www.argo.ucsd.edu>, <http://argo.jcommops.org>) for providing the datasets used in this manuscript. The authors also thank the Ocean Biology Processing Group of NASA for the processing and distribution of MODIS-Aqua data used in this manuscript.

Conflicts of Interest: The authors declare no conflict of interest.

References

- Hirata, T.; Aiken, J.; Hardman-mountford, N.; Smyth, T.J.; Barlow, R.G. Remote Sensing of Environment an absorption model to determine phytoplankton size classes from satellite ocean colour. *Remote Sens. Environ.* **2008**, *112*, 3153–3159. [[CrossRef](#)]
- Karl, D.M. Minireviews: A Sea of Change: Biogeochemical Variability in the North Pacific Subtropical Gyre. *Ecosystems* **1999**, *2*, 181–214. [[CrossRef](#)]
- Longhurst, A. *Ecological Geography of the Sea*; Academic Press: San Diego, CA, USA, 1998.
- Olson, D.M.; Dinerstein, E.; Wikramanayake, E.D.; Burgess, N.D.; Powell, G.V.N.; Underwood, E.C.; D'amico, J.A.; Itoua, I.; Strand, H.E.; Morrison, J.C.; et al. Terrestrial Ecoregions of the World: A New Map of Life on Earth. *Bioscience* **2001**, *51*, 933–938. [[CrossRef](#)]
- Behrenfeld, M.J.; O'Malley, R.T.; Boss, E.S.; Westberry, T.K.; Graff, J.R.; Halsey, K.H.; Milligan, A.J.; Siegel, D.A.; Brown, M.B. Revaluating ocean warming impacts on global phytoplankton. *Nat. Clim. Chang.* **2015**, *6*, 323–330. [[CrossRef](#)]
- Westberry, T.; Behrenfeld, M.J.; Siegel, D.A.; Boss, E. Carbon-based primary productivity modeling with vertically resolved photoacclimation. *Glob. Biogeochem. Cycles* **2008**, *22*. [[CrossRef](#)]
- Aiken, J.; Brewin, R.J.W.; Dufois, F.; Polimene, L.; Hardman-Mountford, N.J.; Jackson, T.; Loveday, B.; Hoya, S.M.; Dall'Olmo, G.; Stephens, J.; et al. A synthesis of the environmental response of the North and South Atlantic Sub-Tropical Gyres during two decades of AMT. *Prog. Oceanogr.* **2016**. [[CrossRef](#)]
- Cullen, J.J. The deep chlorophyll maximum: Comparing vertical profiles of chlorophyll a. *Can. J. Fish. Aquat. Sci.* **1982**, *39*, 791–803. [[CrossRef](#)]
- Kirk, J.T.O. *Light and Photosynthesis in Aquatic Ecosystems*, 3rd ed.; Cambridge University Press: Cambridge, UK, 2011; ISBN 978-0-521-15175-7.
- Grace, J.; San Jose, J.; Meir, P.; Miranda, H.S.; Montes, R.A. Productivity and carbon fluxes of tropical savannas. *J. Biogeogr.* **2006**, *33*, 387–400. [[CrossRef](#)]
- Chisholm, S.W.; Olson, R.J.; Zettler, E.R.; Goericke, R.; Waterbury, J.B. A novel free-living prochlorophyte abundant in the oceanic euphotic zone. *Nature* **1988**, *334*, 340–343. [[CrossRef](#)]
- Bouman, H.A.; Ulloa, O.; Barlow, R.; Li, W.K.W.; Platt, T.; Zvirgmaier, K.; Scanlan, D.J.; Sathyendranath, S. Water-column stratification governs the community structure of subtropical marine picophytoplankton. *Environ. Microbiol. Rep.* **2011**, *3*, 473–482. [[CrossRef](#)] [[PubMed](#)]
- Heywood, J.L.; Zubkov, M.V.; Tarran, G.A.; Fuchs, B.M.; Holligan, P.M. Prokaryoplankton standing stocks in oligotrophic gyre and equatorial provinces of the Atlantic Ocean: Evaluation of inter-annual variability. *Deep Sea Res. II Top. Stud. Oceanogr.* **2006**, *53*, 1530–1547. [[CrossRef](#)]
- Malmstrom, R.R.; Coe, A.; Kettler, G.C.; Martiny, A.C.; Frias-Lopez, J.; Zinser, E.R.; Chisholm, S.W. Temporal dynamics of Prochlorococcus ecotypes in the Atlantic and Pacific oceans. *ISME J.* **2010**, *4*, 1252–1264. [[CrossRef](#)] [[PubMed](#)]
- Rabouille, S.; Edwards, C.A.; Zehr, J.P. Modelling the vertical distribution of Prochlorococcus and Synechococcus in the North Pacific Subtropical Ocean. *Environ. Microbiol.* **2007**, *9*, 2588–2602. [[CrossRef](#)] [[PubMed](#)]
- Zubkov, M.V.; Sleigh, M.A.; Burkill, P.H.; Leakey, R.J.G. Picoplankton community structure on the Atlantic Meridional Transect: A comparison between seasons. *Prog. Oceanogr.* **2000**, *45*, 369–386. [[CrossRef](#)]
- Zubkov, M.V.; Sleigh, M.A.; Tarran, G.A.; Burkill, P.H.; Leakey, R.J.G. Picoplanktonic community structure on an Atlantic transect from 50 degrees N to 50 degrees S. *Deep Sea Res. I Oceanogr. Res. Pap.* **1998**, *45*, 1339–1355. [[CrossRef](#)]

18. Smayda, T.J. Bloom dynamics: Physiology, behavior, trophic effects. *Limnology and Oceanography* **1997**, *42*, 1132–1136. [[CrossRef](#)]
19. Bertilsson, S.; Berglund, O.; Karl, D.M.; Chisholm, S.W. Elemental composition of marine *Prochlorococcus* and *Synechococcus*: Implications for the ecological stoichiometry of the sea. *Limnol. Oceanogr.* **2003**, *48*, 1721–1731. [[CrossRef](#)]
20. Flombaum, P.; Gallegos, J.L.; Gordillo, R.A.; Rincon, J.; Zabala, L.L.; Jiao, N.; Karl, D.M.; Li, W.K.W.; Lomas, M.W.; Veneziano, D.; et al. Present and future global distributions of the marine Cyanobacteria *Prochlorococcus* and *Synechococcus*. *Proc. Natl. Acad. Sci. USA* **2013**, *110*, 9824–9829. [[CrossRef](#)] [[PubMed](#)]
21. Williams, R.G.; Follows, M.J. Biological Fundamentals. In *Ocean Dynamics and the Carbon Cycle: Principles and Mechanisms*; Williams, R.G., Follows, M.J., Eds.; Cambridge University Press: New York, NY, USA, 2011.
22. *NASA Moderate Resolution Imaging Spectroradiometer (MODIS-Aqua) Ocean Color Data*; Goddard Space Flight Center Ocean Biology Processing Group: Greenbelt, MD, USA, 2014.
23. Gordon, H.R.; Morel, A.Y. *Remote Assessment of Ocean Color for Interpretation of Satellite Visible Imagery*; Springer-Verlag New York: New York, USA, 1983.
24. Hosoda, S.; Ohira, T.; Nakamura, T. A monthly mean dataset of global oceanic temperature and salinity derived from Argo float observations. *JAMSTEC Rep. Res. Dev.* **2008**, *8*, 47–59. [[CrossRef](#)]
25. Johnson, Z.I.; Zinser, E.R.; Coe, A.; McNulty, N.P.; Woodward, E.M.; Chisholm, S.W. Niche Partitioning Among *Prochlorococcus* Ecotypes Along Ocean-Scale Environmental Gradients. *Science* **2006**, *311*, 1737–1740. [[CrossRef](#)] [[PubMed](#)]
26. Zinser, E.R.; Johnson, Z.I.; Coe, A.; Karaca, E.; Veneziano, D.; Chisholm, S.W. Influence of light and temperature on *Prochlorococcus* ecotype distributions in the Atlantic Ocean. *Limnol. Oceanogr.* **2007**, *52*, 2205–2220. [[CrossRef](#)]
27. Platt, T.; Gallegos, C.L.; Harrison, W.G. Photoinhibition of photosynthesis in natural assemblages of marine phytoplankton. *J. Mar. Res.* **1980**, *38*, 687–701.
28. De Boyer Montégut, C.; Madec, G.; Fischer, A.S.; Lazar, A.; Iudicone, D. Mixed layer depth over the global ocean: An examination of profile data and a profile-based climatology. *J. Geophys. Res. Oceans* **2004**, *109*, 1–20. [[CrossRef](#)]
29. Morel, A.; Berthon, J.-F. Surface pigments, algal biomass profiles, and potential production of the euphotic layer: Relationships reinvestigated in view of remote-sensing applications. *Limnol. Oceanogr.* **1989**, *34*, 1545–1562. [[CrossRef](#)]
30. Venables, W.N.; Ripley, B.D. *Modern Applied Statistics with S*, 4th ed.; Springer: New York, NY, USA, 2002; Volume 53, ISBN 0387954570.
31. Brewin, R.J.W.; Sathyendranath, S.; Müller, D.; Brockmann, C.; Deschamps, P.Y.; Devred, E.; Doerffer, R.; Fomferra, N.; Franz, B.; Grant, M.; et al. The Ocean Colour Climate Change Initiative: III. A round-robin comparison on in-water bio-optical algorithms. *Remote Sens. Environ.* **2015**, *162*, 271–294. [[CrossRef](#)]
32. Forsythe, W.C.; Rykiel, E.J.; Stahl, R.S.; Wu, H.I.; Schoolfield, R.M. A model comparison for daylength as a function of latitude and day of year. *Ecol. Model.* **1995**, *80*, 87–95. [[CrossRef](#)]
33. Cooper, P.I. The absorption of radiation in solar stills. *Sol. Energy* **1969**, *12*, 333–346. [[CrossRef](#)]
34. Biller, S.J.; Berube, P.M.; Lindell, D.; Chisholm, S.W. *Prochlorococcus*: The structure and function of collective diversity. *Nat. Rev. Microbiol.* **2014**, *13*, 13–27. [[CrossRef](#)] [[PubMed](#)]
35. McClain, C.R.; Signorini, S.R.; Christian, J.R. Subtropical gyre variability observed by ocean-color satellites. *Deep Sea Res. II Top. Stud. Oceanogr.* **2004**, *51*, 281–301. [[CrossRef](#)]
36. Brew, H.S.; Moran, S.B.; Lomas, M.W.; Burd, A.B. Plankton community composition, organic carbon and thorium-234 particle size distributions, and particle export in the Sargasso Sea. *J. Mar. Res.* **2009**, *67*, 845–868. [[CrossRef](#)]
37. Behrenfeld, M.J.; Falkowski, P.G. Photosynthetic rates derived from satellite-based chlorophyll concentration. *Limnol. Oceanogr.* **1997**, *42*, 1–20. [[CrossRef](#)]
38. Babin, M.; Theriault, J.C.; Legendre, L.; Nieke, B.; Reuter, R.; Condal, A. Relationship between the maximum quantum yield of carbon fixation and the minimum quantum yield of chlorophyll a in vivo fluorescence in the Gulf of St. Lawrence. *Limnol. Oceanogr.* **1995**, *40*, 956–968. [[CrossRef](#)]
39. Tsubouchi, T.; Suga, T.; Hanawa, K. Comparison study of subtropical mode waters in the world ocean. *Front. Mar. Sci.* **2016**, *3*, 270. [[CrossRef](#)]
40. Boggs, S.W. This Hemisphere. *J. Geol.* **1945**, *44*, 345–355. [[CrossRef](#)]

41. Dave, A.C.; Barton, A.D.; Lozier, M.S.; McKinley, G.A. What drives seasonal change in oligotrophic area in the subtropical North Atlantic? *J. Geophys. Res. Oceans* **2015**, *120*, 3958–3969. [[CrossRef](#)]
42. Polovina, J.J.; Howell, E.A.; Abecassis, M. Ocean's least productive waters are expanding. *Geophys. Res. Lett.* **2008**, *35*, L03618. [[CrossRef](#)]
43. Durand, M.D.; Olson, R.J.; Chisholm, S.W. Phytoplankton population dynamics at the Bermuda Atlantic Time-series station in the Sargasso Sea. *Deep Sea Res. II Top. Stud. Oceanogr.* **2001**, *48*, 1983–2003. [[CrossRef](#)]
44. Barton, A.D.; Ward, B.A.; Williams, R.G.; Follows, M.J. The impact of fine-scale turbulence on phytoplankton community structure. *Limnol. Oceanogr. Fluids Environ.* **2014**, *4*, 34–49. [[CrossRef](#)]
45. Buitenhuis, E.T.; Li, W.K.W.; Vault, D.; Lomas, M.W.; Landry, M.R.; Partensky, F.; Karl, D.M.; Ulloa, O.; Campbell, L.; Jacquet, S.; et al. Picophytoplankton biomass distribution in the global ocean. *Earth Syst. Sci. Data* **2012**, *4*, 37–46. [[CrossRef](#)]
46. Mella-Flores, D.; Six, C.; Ratin, M.; Partensky, F.; Boutte, C.; Le Corguillé, G.; Marie, D.; Blot, N.; Gourvil, P.; Kolowrat, C.; Garczarek, L. Prochlorococcus and synechococcus have evolved different adaptive mechanisms to cope with light and uv stress. *Front. Microbiol.* **2012**, *3*, 285. [[CrossRef](#)] [[PubMed](#)]
47. Partensky, F.; Hess, W.R.; Vault, D. Prochlorococcus, a marine photosynthetic prokaryote of global significance. *Microbiol. Mol. Biol. Rev.* **1999**, *63*, 106–127. [[PubMed](#)]



© 2018 by the authors. Licensee MDPI, Basel, Switzerland. This article is an open access article distributed under the terms and conditions of the Creative Commons Attribution (CC BY) license (<http://creativecommons.org/licenses/by/4.0/>).